Sensorless Control of Five-phase PMSM Drives Post the failure in two phases.

Kamel Saleh[a]* and M. Sumner[b]

[a]Electrical Engineering Dept, An-Najah National University, Nablus, Palestine;
[b]Electrical Engineering Dept, Nottingham University, Nottingham, UK
*kamel.saleh@najah.edu. mark.sumner@nottingham.ac.uk

Abstract

This paper introduces a novel technique to maintain the operation of the five-phase Permanent Magnet Synchronous Motor (PMSM) post the failure in two phases of the motor and post the failure of the speed sensor occurs simultaneously. To achieve that, Firstly, a Fault Tolerant Control (FTC) technique is implemented. The FTC is based on implementing two new Space Vector Pulse Width Modulation (SVPWM) besides using Field Oriented Control (FOC) to minimize the Torque ripple and to maintain the performance post the two-phase failure. Secondly, Algorithms are proposed to obtain the saliency position post the failure of the two phases. The Technique is based on measuring the transient response of the motor's remaining healthy currents due to the inverter switching actions. These switching actions are related to the PWM signals obtained from the new SVPWM techniques implemented post the two-phase failure. The whole control technique post the failures is very simple to implement. Simulation results are provided to verify the reliability of the proposed control technique to maintain the performance of the five-phase motor drive post the failure in the two phases and the failure of the speed sensor occurred simultaneously without compromising the preperformance (maintain the torque ripple less than 3.6 % and 3.4% post the failure). Moreover, the results have demonstrated the ability for the whole system to work effectively over a wide speed range and load conditions post the failure.

Keywords: five-phase PMSM motor, SVPWM, open-circuit faults, Sensorless Control. FOC

1. Introduction

Multi-phase machines have witnessed an increased interest in many industrial applications [1-2] due to the increasing demand for a highly reliable electrical drive. Compared to the three-phase configuration, multi-phase machines offer the intrinsic advantages of higher power density, lower torque pulsation, and better fault-tolerance

During the normal operating conditions, multi-dimension SVPWM can be utilized in a multi-phase motor drive to cancel the third harmonic in the stator currents to enhance the torque [3-6]. In the cases of a failure in one phase or two phases of the five-phase motor drive, a fault-tolerant control (FTC) strategy should be adopted to control the remaining current to obtain a minimum torque ripple, equal phase currents, and minimum copper losses [7-9]. In these cases, the traditional PWM techniques become inapplicable due to the unbalance in voltages and currents of the five-phase motor post the failure. Hence, hysteresis current controller has been implemented post the failure to control the remaining currents according to the FTC strategy [8-10]. However, the switching frequency in the hysteresis control is inconstant and that limits its use in industrial applications. To avoid the use of hysteresis control, modified SVPWM strategies for five-phase motor under one phase failure are used [11-12]. To realize Vector Control (VC) operation post the failure in a single phase, and two phases, transformation matrices are introduced [13-17] and [18-20] respectively. Other Techniques were used such as Direct-Torque Control (DTC) [21], Sliding Mode Control [22], Model predictive control [23] to control the remaining healthy currents to minimize the torque post the failure.

Sensorless control of five-phase motor running under normal operating conditions has been researched in the last couple of years. This research is focusing on model-based sensorless control, direct torque control, and high-frequency injections [24–27].

Recently, few papers were presented the sensorless control of the five-phase motor post the failure in one phase [28-29]. To the author's best knowledge, No paper has introduced the sensorless control of the five-phase motor under two-phase failure yet.

The major contribution of this paper is that it is the first paper that presents a fault-tolerant five drive system that can maintain the operation post the failure two phases of the motor and post the failure in the speed sensor occurs. This improvement in the reliability of the drive system is related to using two strategies during the fault. The first strategy is to implement a new FTC strategy to maintain the operation of the motor post the failure in the two phases. The FTC is based on implementing two new Space Vector Pulse Width Modulation (SVPWM). This strategy helps to maintain the torque ripple less than 3.4% post the fault. The second strategy is to implement new algorithms to obtain the saliency position based on the new

FTC strategy. The whole control technique post the failures is very simple to implement and has a performance as good as the performance of the system under healthy operating conditions.

2. *Five-phase PMSM drive*

Figure 1 illustrates the five-phase PMSM drive topology [30]. The PMSM motor is modeled according to equations (1--5).

$$
\begin{bmatrix} v_A \\ v_B \\ v_C \\ v_D \\ v_E \end{bmatrix} = r_s * \begin{bmatrix} i_A \\ i_B \\ i_C \\ i_D \\ i_E \end{bmatrix} + \begin{bmatrix} d\phi_A/dt \\ d\phi_B/dt \\ d\phi_C/dt \\ d\phi_D/dt \\ d\phi_E/dt \end{bmatrix} \quad (1)
$$

$$
\begin{bmatrix} \phi_A \\ \phi_B \\ \phi_C \\ \phi_D \\ \phi_E \end{bmatrix} = \begin{bmatrix} L_{AA} & L_{AB} & L_{AC} & L_{AD} & L_{AE} \\ L_{AB} & L_{BB} & L_{BC} & L_{BD} & L_{BE} \\ L_{AC} & L_{BC} & L_{CC} & L_{CD} & L_{CE} \\ L_{AD} & L_{BD} & L_{CD} & L_{DD} & L_{DE} \\ L_{AE} & L_{BE} & L_{CE} & L_{DE} & L_{EE} \end{bmatrix} \begin{bmatrix} i_A \\ i_B \\ i_C \\ i_D \\ i_E \end{bmatrix} + \begin{bmatrix} \varphi_{mA} \\ \varphi_{mB} \\ \varphi_{mC} \\ \varphi_{mD} \\ \varphi_{mE} \end{bmatrix} \quad (2)
$$

Where $v_{A,B,C,D,E}$ are the stator voltages, r_s is the stator resistance, $i_{A,B,C,D,E}$ are the stator currents, $\phi_{A,B,C,D,E}$ are the stator linking fluxes, L_{AA}, L_{BB}, L_{CC}, L_{DD} and L_{EE} are the total stator self-inductances, and L_{AB}, L_{AC}, L_{BA}, L_{AD}, L_{AE}, L_{BC}, L_{BD}, L_{BE}, L_{CD}, L_{CE} and L_{DE} are the total stator mutual inductances. $\varphi_{mA,B,C,D,E}$ are the permanent magnet fluxes.

The stator total self and mutual inductances are dependent on rotor angle as shown below:-

$$
\begin{bmatrix} L_{AA} \\ L_{BB} \\ L_{CC} \\ L_{DD} \\ L_{EE} \end{bmatrix} = \begin{bmatrix} L_{so} + L_{sl} \\ L_{so} + L_{sl} \\ L_{so} + L_{sl} \\ L_{so} + L_{sl} \\ L_{so} + L_{sl} \end{bmatrix} + L_x * \begin{bmatrix} \cos(2\theta_r) \\ \cos(2\theta_r - 2\theta_x) \\ \cos(2\theta_r - 4\theta_x) \\ \cos(2\theta_r - 6\theta_x) \\ \cos(2\theta_r - 8\theta_x) \end{bmatrix} \quad (3),
$$

$$
\begin{bmatrix} L_{AB} \\ L_{AC} \\ L_{AD} \\ L_{AE} \\ L_{BC} \\ L_{BD} \\ L_{BE} \\ L_{CD} \\ L_{CE} \\ L_{DE} \end{bmatrix} = L_{so} * \begin{bmatrix} \cos(\theta_x) \\ \cos(2\theta_x) \\ \cos(3\theta_x) \\ \cos(4\theta_x) \\ \cos(\theta_x) \\ \cos(2\theta_x) \\ \cos(2\theta_x) \\ \cos(\theta_x) \\ \cos(2\theta_x) \\ \cos(\theta_x) \end{bmatrix} + L_x * \begin{bmatrix} \cos(2\theta_r - 2\theta_x) \\ \cos(2\theta_r - 4\theta_x) \\ \cos(2\theta_r - 6\theta_x) \\ \cos(2\theta_r + 8\theta_x) \\ \cos(2\theta_r - 6\theta_x) \\ \cos(2\theta_r - 8\theta_x) \\ \cos(2\theta_r) \\ \cos(2\theta_r) \\ \cos(2\theta_r - 2\theta_x) \\ \cos(2\theta_r - 4\theta_x) \end{bmatrix} \quad (4)
$$

where: L_{so} and , L_{sl} is the stator mutual and self inductance. L_x is the stator inductance fluctuation, and θ_x is $\pi/5$. both stator self and mutual inductance are modulated by saturation saliency that appears in the term $(2\theta_r)$. The stator flux-linkages due to the permanent magnet are

$$
\begin{bmatrix} \varphi_{mA} \\ \varphi_{mB} \\ \varphi_{mC} \\ \varphi_{mD} \\ \varphi_{mE} \end{bmatrix} = \Lambda_m * \begin{bmatrix} \cos(\theta_r) \\ \cos(\theta_r - 2\theta_x) \\ \cos(\theta_r - 4\theta_x) \\ \cos(\theta_r - 6\theta_x) \\ \cos(\theta_r - 8\theta_x) \end{bmatrix} \quad (5),
$$

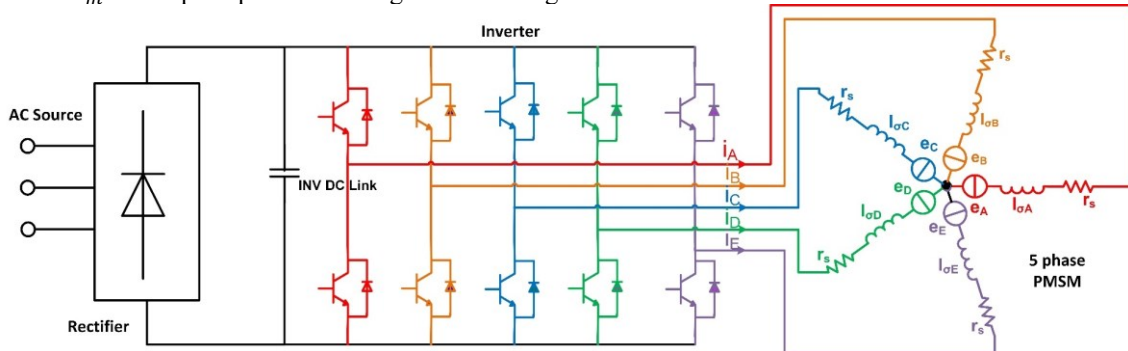where Λ_m is the peak permanent magnet flux linkage.

Figure 1. Five-phase PMSM Drive.

2.1 Currents of the five-phase motor post the failure

Five-phase motor drives are potentially fault-tolerant as mentioned previously. By utilizing a proper FTC strategy, the five-phase motor can maintain its operation with minimum torque ripple even post a two-phase failure. The FTC should maintain the torque-producing MMF without the need to use a neutral line to ensure safe operation.

Under the normal operating conditions, the currents of the five-phase motor are given in equation (6) and figure 2 [6,31-35]:

$$\begin{bmatrix} i_A \\ i_B \\ i_C \\ i_D \\ i_E \end{bmatrix} = \begin{bmatrix} I_m * \cos(wt) \\ I_m * \cos(wt - 2\theta_x) \\ I_m * \cos(wt - 4\theta_x) \\ I_m * \cos(wt + 4\theta_x) \\ I_m * \cos(wt + 2\theta_x) \end{bmatrix} \quad (6)$$
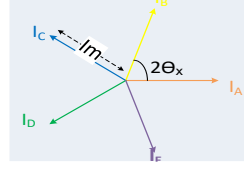

Figure 2 five-phase motor currents under normal operating condition

Where I_m is the amplitude of the phase current.

If phase 'A' is opened as an example [6], the performance of the five-phase motor can be maintained by setting the current in phase 'A' to zero and assuming that :

$$i'_B = -i'_D \ , i'_C = -i'_E \quad (7)$$

Where i'_B , i'_C , i'_D , and i'_E are the remaining currents in phase 'B' , 'C', 'D', and 'E' post the failure in phase 'A'.

The currents i'_B , i'_C , i'_D , and i'_E can calculated by:-

$$i'_B = -i'_D = \frac{5I_m}{4(\sin(\theta_x))^2}\cos(wt - \theta_x) \ , i'_D = -i'_E = \frac{5I_m}{4(\sin(\theta_x))^2}\cos(wt - 4\theta_x) \quad (8)$$

This means that to maintain the performance of the five-phase motor post the failure in one phase, the remaining currents should be to be increased by 1.382 times the current under the normal operating condition as shown in equation 9 and figure 3. Also, the currents besides the faulted phase should be shifted $(\pi/5)$ towards the faulted phase.

$$\begin{bmatrix} I'_A \\ I'_B \\ I'_C \\ I'_D \\ I'_E \end{bmatrix} = \begin{bmatrix} 0 \\ 1.382 * I_m * \cos(wt - \theta_x) \\ 1.382 * I_m * \cos(wt - 4\theta_x) \\ 1.382 * I_m * \cos(wt - 6\theta_x) \\ 1.382 * I_m * \cos(wt - 9\theta_x) \end{bmatrix} \quad (9)$$
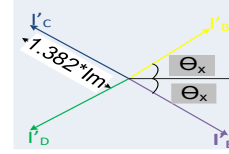

Figure 3 five-phase motor currents post a failure in phase 'A'.

In the same way, when the two adjacent phases 'a' and 'b' are opened, the performance of the five-phase motor can be maintained assuming that the neutral current is zero [6]. And hence the remaining currents in the phases 'c', 'd', and 'e' post the failure can be calculated as follows:-

$$i''_c = \frac{5I_m \cos(\theta_x)}{2(\sin(2\theta_x))^2}\cos(wt - 2\theta_x), i''_d = \frac{5I_m \cos(\theta_x)^2}{(\sin(2\theta_x))^2}\cos(wt - 4\theta_x), i''_e = \frac{5I_m \cos(\theta_x)}{2(\sin(2\theta_x))^2}\cos(wt) \quad (10)$$

This means that to maintain the performance of the five-phase motor post the failure in the two adjacent phases 'A' and 'B'. The remaining current in phase 'D' should be increased by 3.618 times compared to its value under the normal operating conditions while the remaining current in phases 'C' and 'E' should be increased by 2.236 times. Moreover, the remaining current in phase 'C' and 'E' should be shifted $(2\pi/5)$ towards the faulted phases 'A' and 'B' respectively as shown in equation 11 and figure 4.

$$\begin{bmatrix} I''_A \\ I''_B \\ I''_C \\ I''_D \\ I''_E \end{bmatrix} = \begin{bmatrix} 0 \\ 0 \\ 2.236 * I_m * \cos(wt - 2\theta_x) \\ 3.618 * I_m * \cos(wt + 4\theta_x) \\ 2.236 * I_m * \cos(wt) \end{bmatrix} \quad (11)$$
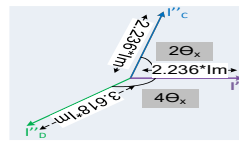

Figure 4 five-phase motor currents post the failure in the two adjacent phases adjacent phases 'A' and 'B' .

Finally, when the two nonadjacent phases 'B' and 'E' are opened, the performance of the five-phase motor can be maintained assuming that the neutral current is zero. And hence the remaining currents in the phases 'A', 'C', and 'D' post the failure can be calculated as follows:-

$$i''_A = \frac{5I_m}{4(\sin(2\theta_x))^2}\cos(wt), i''_C = \frac{5I_m}{8(\sin(2\theta_x))^2 \cos(3\theta_x)}\cos(wt - 3\theta_x),$$

$$i''_D = \frac{5I_m}{8(\sin(2\theta_x))^2 \cos(2\theta_x)}\cos(wt + 3\theta_x) \quad (12)$$

This means that to maintain the performance of the five-phase motor post the failure in the two nonadjacent phases 'B' and 'E'. The remaining current in phase 'A' should be increased by 1.382 times compared to its value under the normal operating condition while the remaining current in phases 'C' and 'D' should be

increased by 2.236 times. Moreover, the remaining current in phases 'C' and 'D' should be shifted $(\pi/5)$ towards the faulted phases 'B' and 'E' respectively as shown in equation 13 and figure 5.

$$\begin{bmatrix} I''_A \\ I''_B \\ I''_C \\ I''_D \\ I''_E \end{bmatrix} = \begin{bmatrix} 1.382 * I_m * \cos(wt) \\ 0 \\ 2.236 * I_m * \cos(wt - 3\theta_x) \\ 2.236 * I_m * \cos(wt + 3\theta_x) \\ 0 \end{bmatrix} (13)$$
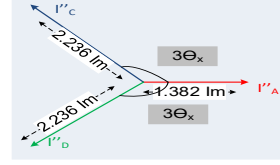

Figure 5 five-phase motor currents post the failure in the two nonadjacent phases adjacent phases 'A' and 'B'.

2.2 SVPWM of the Fault -Tolerant PMSM

2.2.1   SVPWM under healthy operating condition

To regulate the currents according to equation (6), multi-Dimension SVPWM can be used [3-6].   In this method, two stationary frames α1-β1 and α3-β3 were used to map the fundamental component and the third harmonic component respectively of the reference voltage (V_ref) as shown in Figures 6.a and 6.b respectively.
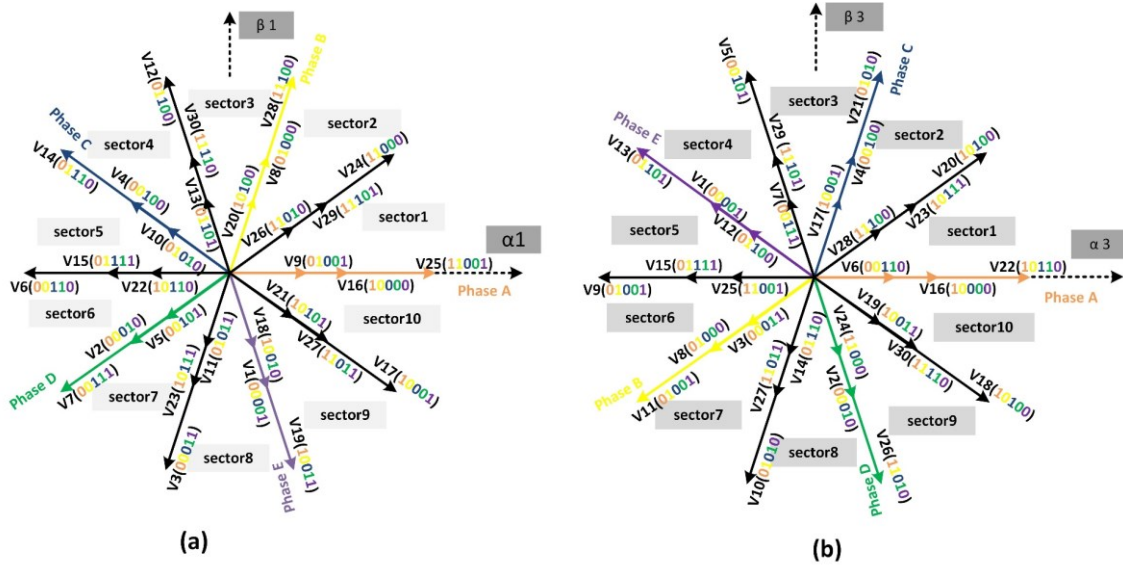

Figure 6. Vector diagram of the all the vectors in (a) α1 –β1 plane and (b) α3 –β3 plane in multi-dimension SVPWM.

2.2.2   SVPWM post a failure in phase 'A'.

To regulate the currents according to equation (9) post a failure in phase 'A', the asymmetric SVPWM method can be implemented [12]. This method depends on a reconstruction of the space vector diagram post the failure based on the distribution of the stator currents post the failure in phase 'A' according to the FTC strategy as shown in figure 7.
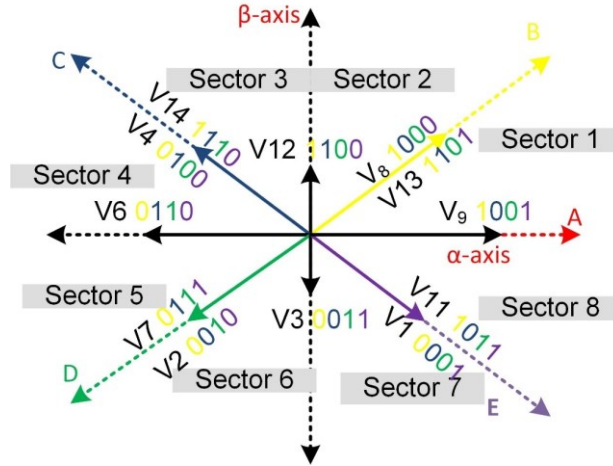
Figure 7. switching vectors on a-β axis of asymmetric SVPWM post the failure in phase 'A'.

2.2.3   SVPWM post a failure in the adjacent phases 'A' and 'B'

To regulate the currents according to equation (11) post the failure in the adjacent phases 'A' and 'B', a novel SVPWM method is presented in this paper. This method depends on a reconstruction of the space vector diagram post the failure in the adjacent phases 'A' and 'B' of the five-phase motor based on the changes of the healthy remaining currents as shown in figure 8.

The vectors in figure 8 can be categorized into two groups according to their amplitudes. The first group consists of the vectors V1, V3, V4, and V6 with amplitude equals 0.4*VDC. The second group consists of the vectors V3, and V5 with amplitude equals 1.618*0.4*VDC.
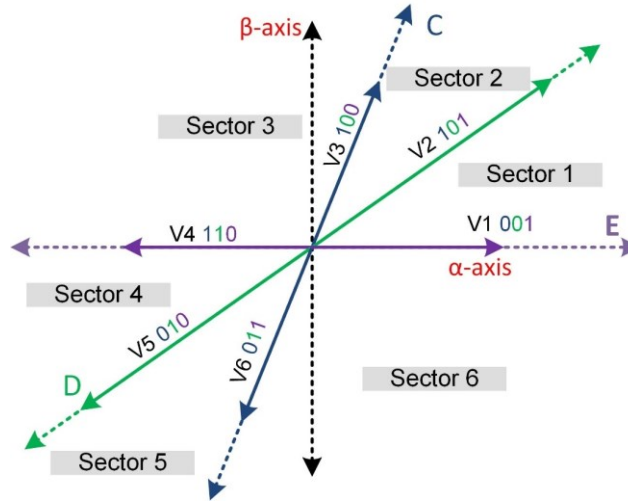
Figure 8 switching vectors on a-β axis of a new SVPWM post a failure in adjacent phases 'A' and 'B'.

The algorithm to implement the new SVPWM post a failure in the adjacent phases 'A' and 'B' is given in table 1 and table 2. More illustrations about the new SVPWM can be found in the appendix.

Table 1. Selection of the Sector.

Angle of reference voltage (θ)	Sector number
$0 \leq \theta < \theta_x$	1
$\theta_x \leq \theta < 2\theta_x$	2
$2\theta_x \leq \theta < 5\theta_x$	3
$5\theta_x \leq \theta < 6\theta_x$	4
$6\theta_x \leq \theta < 7\theta_x$	5
$7\theta_x \leq \theta < 10\theta_x$	6

Table 2: Dwell time calculation and switch sequence in new SVPWM post failure in adjacent phases 'a' and

Sector	T1	T2	T0	Switching sequence

1	$\dfrac{V_\alpha - 1.3764*V_\beta}{0.4*VDC}*Ts$	$\dfrac{1.0515*V_\beta}{0.4*VDC}*Ts$	$Ts - T1 - T2$	$V1, V2, V0$
2	$\dfrac{-V_\alpha + 1.3764*V_\beta}{0.4*VDC}*Ts$	$\dfrac{V_\alpha - 0.3249*V_\beta}{0.4*VDC}*Ts$	$Ts - T1 - T2$	$V3, V2, V0$
3	$\dfrac{1.0515*V_\beta}{0.4*VDC}*Ts$	$\dfrac{-V_\alpha + 0.3249*V_\beta}{0.4*VDC}*Ts$	$Ts - T1 - T2$	$V3, V4, V0$
4	$\dfrac{-1.0515*V_\beta}{0.4*VDC}*Ts$	$\dfrac{-V_\alpha + 1.3764*V_\beta}{0.4*VDC}*Ts$	$Ts - T1 - T2$	$V5, V4, V0$
5	$\dfrac{-V_\alpha + 1.3764*V_\beta}{0.4*VDC}*Ts$	$\dfrac{V_\alpha - 1.3764*V_\beta}{0.4*VDC}*Ts$	$Ts - T1 - T2$	$V5, V6, V0$
6	$\dfrac{V_\alpha - 0.3249*V_\beta}{0.4*VDC}*Ts$	$\dfrac{-1.0515*V_\beta}{0.4*VDC}*Ts$	$Ts - T1 - T2$	$V1, V6, V0$

2.2.4   SVPWM post a failure in the non-adjacent phases 'B' and 'E'

To regulate the currents according to equation (13) post a failure in the non-adjacent phases 'B' and 'E', a novel SVPWM method is presented in this paper. This method depends on the reconstruction of the space vector diagram post the failure in the non-adjacent phases 'B' and 'E' of the five-phase motor based on the changes in the remaining healthy currents as shown in figure 9.

Figure 9 switching vectors on a-ß axis of a new SVPWM post a failure in the non-adjacent phases 'B' and 'E'

The vectors in figure 9 can be categorized into two groups according to their amplitude. The first group consists of the vectors V1, and V4 with amplitude equals 0.4*VDC. The second group consists of the vectors V2, V3, V5, and V6 with amplitude equals 1.618*0.4*VDC.
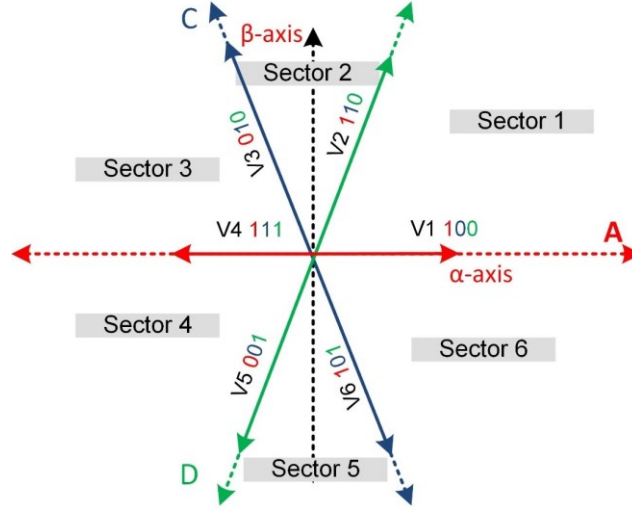The algorithm to implement the SVPWM post a failure in the non-adjacent phases 'B' and 'E' is given in table 3 and table 4.

Table 3. Selection of the Sector.

Angle of reference voltage (θ)	Sector number
$0 \leq \theta < 2\theta_x$	1
$2\theta_x \leq \theta < 3\theta_x$	2
$3\theta_x \leq \theta < 5\theta_x$	3
$5\theta_x \leq \theta < 7\theta_x$	4
$7\theta_x \leq \theta < 8\theta_x$	5
$8\theta_x \leq \theta < 10\theta_x$	6

Table 4: Dwell time calculation in new SVPWM in case of a failure in phases 'b' and 'e'

Sector	T1	T2	T0	Switching sequence
1	$\dfrac{V_\alpha - 0.325*V_\beta}{0.4*VDC}*Ts$	$\dfrac{0.65*V_\beta}{0.4*VDC}*Ts$	$Ts - T1 - T2$	$V1, V2, V0$

2	$\dfrac{-V_\alpha + 0.325*V_\beta}{0.4*VDC} * Ts$	$\dfrac{V_\alpha + 0.325*V_\beta}{0.4*VDC} * Ts$	$Ts - T1 - T2$	$V3, V2, V0$
3	$\dfrac{0.65*V_\beta}{0.4*VDC} * Ts$	$\dfrac{-V_\alpha - 0.325*V_\beta}{0.4*VDC} * Ts$	$Ts - T1 - T2$	$V3, V4, V0$
4	$\dfrac{-0.65*V_\beta}{0.4*VDC} * Ts$	$\dfrac{-V_\alpha + 0.325*V_\beta}{0.4*VDC} * Ts$	$Ts - T1 - T2$	$V5, V4, V0$
5	$\dfrac{-V_\alpha - 0.325*V_\beta}{0.4*VDC} * Ts$	$\dfrac{V_\alpha - 0.325*V_\beta}{0.4*VDC} * Ts$	$Ts - T1 - T2$	$V5, V6, V0$
6	$\dfrac{V_\alpha + 0.325*V_\beta}{0.4*VDC} * Ts$	$\dfrac{-0.65*V_\beta}{0.4*VDC} * Ts$	$Ts - T1 - T2$	$V1, V6, V0$

2.2.5   Simulation results for the PMSM motor drive post the failure in two phases.

The multi-dimension SVPWM, asymmetric SVPWM, in addition to the new SVPWM techniques proposed in this paper has been simulated in the SABER as shown in figure 10. Multi-dimension SVPWM will be used under the normal operating conditions. If a failure in phase 'A' has occurred, the asymmetric SVPWM technique will be used. The SVPWM techniques proposed in section 2.3.3 will be used if a failure in the two adjacent phases 'A' and 'B' has occurred. Finally, the SVPWM proposed in section 2.3.4 will be used if a failure in the two nonadjacent phases 'B' and 'E' is introduced. It should be mentioned here that the faults are introduced in predefined times, and no algorithms were used to detect the fault.
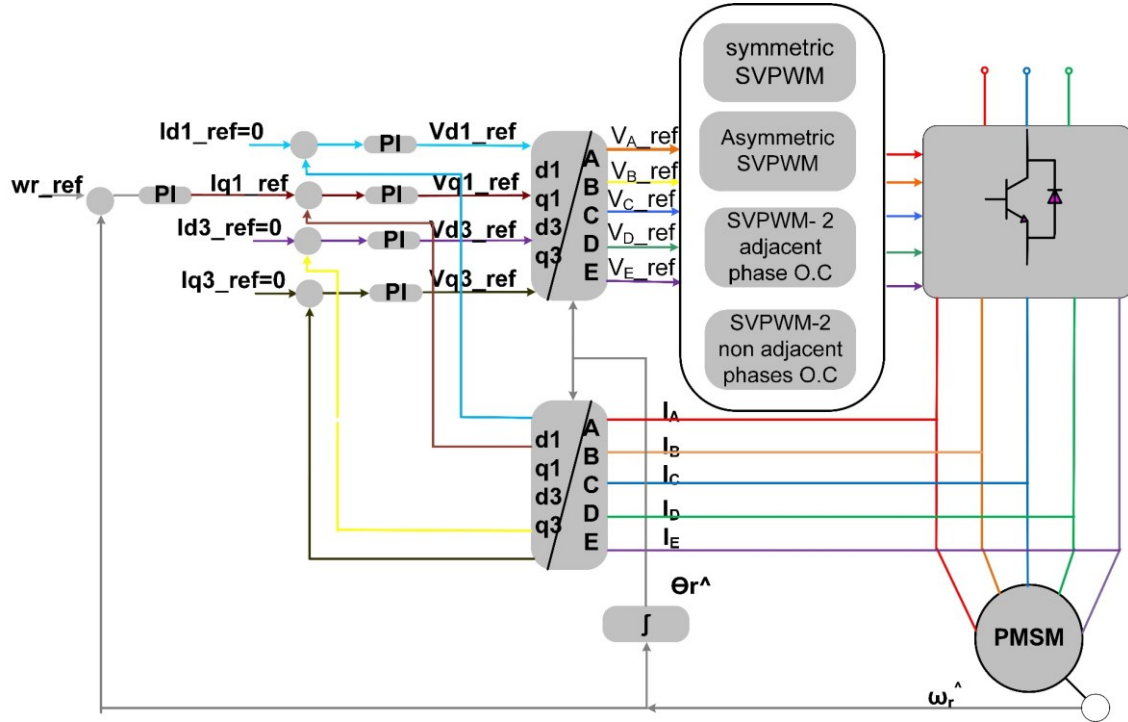

Figure 10 Speed control structure of five-phase motor drive post the failure in phases.

The simulation results obtained from implementing the FOC scheme illustrated in figure 10 are shown in figure 11. The motor was running at 250 rpm and 50% load under the normal operating conditions during the time periods [1.5s-2s], [2.5s-3s], and [3.5s-4s].   The stator currents in these periods were equal in magnitude and phase-shifted by 72° similar to those given in equation (6). During the time period [2s-2.5s], a failure occurred in phase 'A' of the PMSM. Hence, the asymmetric SVPWM was utilized. The results illustrate the fact that the remaining motor currents in this period were increased by 1.382 times their values under the normal operating conditions. Moreover, the results illustrate that the currents in the phases 'B' and 'E' were shifted by 36° towards the failure phase 'A'. These results agree completely with equation (9). After that, During the time period [3s-3.5s], a failure in the adjacent phases 'A' and 'B' occurred, and at the same time, the new SVPWM technique presented in section 2.3.3 was implanted. Many observations can be mentioned based on the results. Firstly: the current in phase 'D' was increased by 3.618 times its value under the normal operating conditions while the currents in phases 'C' and 'E' were also increased

by 2.236 times. Secondly, the current in phase 'C' was shifted by 72° to replace the failure phase 'B' while the current in phase 'E' is shifted by 72° towards the failure phase 'A'. These observations agree completely with equation (11). Finally, during the time period [4s-4.5s], The non-adjacent phases 'B' and 'E' were exposed to a failure and at the same time, the new SVPWM technique presented in section 2.3.4 was implanted. Many points can be noticed from the current waveforms in this interval. Firstly: the current in phase 'A' was increased by 1.382 times its value under the normal operating conditions while the current in phases 'C' and 'D' were also increased by 2.236 times. Secondly, the current in phase 'C' was shifted by 36° towards the failure phase 'B' while the current in phase 'D' is shifted by 36° towards the failure phase 'E'. These observations agree completely with equation (13). The most important thing that can be demonstrated from the result is that the ripple in speed and torque was minimum and almost negligible even at extreme cases when the two phases of the motor were exposed to failure. It should be mentioned here that the currents in healthy phases post the fault will increase by 3.618 and 2.236 times which will increase the temperature of the motor if it lasts for a long time. And hence, the operation of the motor post the fault should be restricted for a short time.
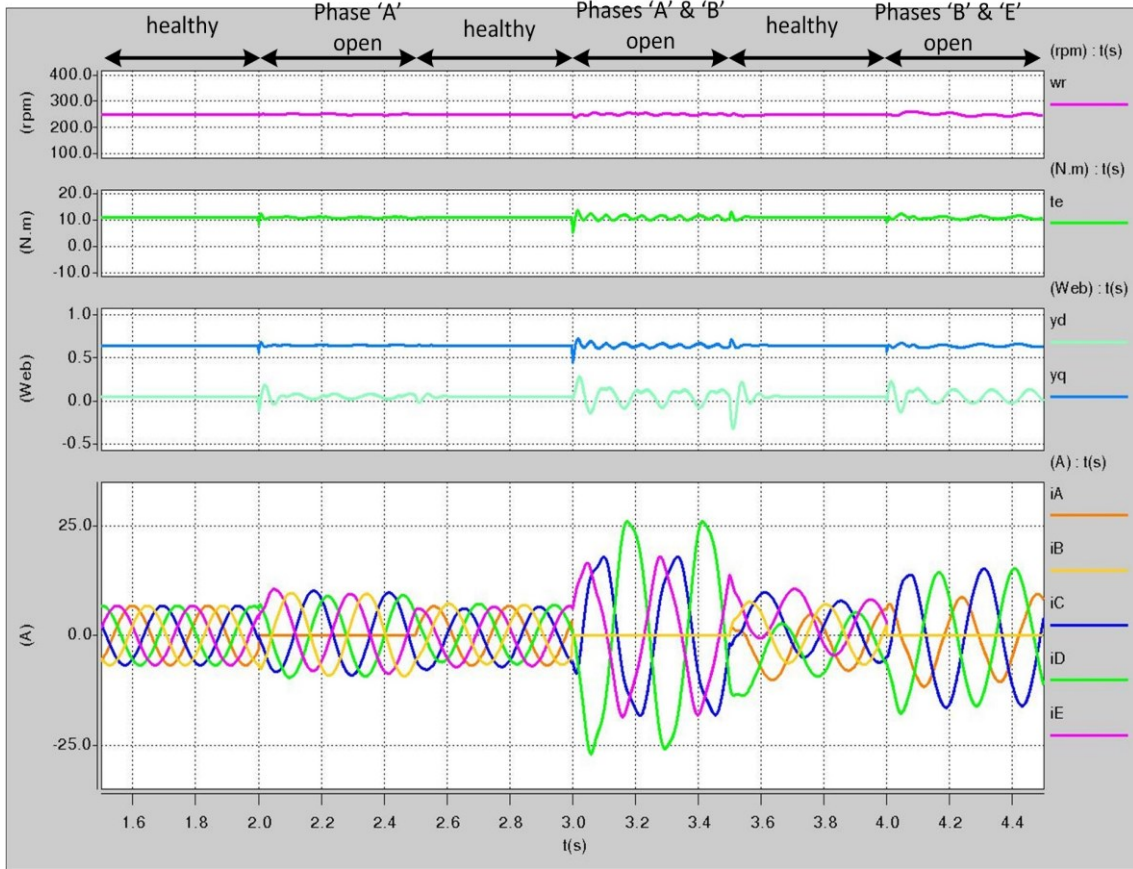

Figure 11: simulation results of the five-phase motor drive post the failure in phases.

2.3 Saliency position track post the failure

The algorithm to obtain the saliency position while the motor is running under the normal operating conditions can't be used post the failures [36-37] as shown in figure 12. During the periods [1s-2s], [3s-4s], and [5s-6s], the motor was running under the normal operating conditions and the results given in figure 12 illustrates that saliency position could be obtained properly. During the periods [2s-3s],[4s-5s], and [6s-7s] the positions scalar couldn't be obtained as a failure in phase 'A', failure in the adjacent phase 'A' and 'B', and failure in the nonadjacent phase 'B' and 'E' have occurred respectively. This is related to the fact that the saliency position scalars are obtained through measuring the transient responses of phase current of the five-phase motors and the currents 'A', 'B', and 'E' are zero in these time intervals due to the failure. Moreover, the PWM signals will change according to the type of fault and hence, the sampling time of the transient current response that is related to the PWM waveform will change also that will lead to the zero position scalars.

It should be mentioned that the papers [38-39] have presented a new algorithm to obtain the saliency position post the failure in one phase. But yet, no paper deals with saliency tracking post the failure in two phases.

2.3.1   tracking the saliency post the failure in the adjacent phases 'A' and 'B'

Figure 13 shows the proposed SVPWM and the PWM waveform that is used as a part of the FTC strategy post the failure in the two adjacent phases 'A' and 'B' of the five-phase motor when the V_ref is located in the first sector.
Figures 14a, 14.b , 14.c, and 14.d show the stator circuits of five-phase PM motor post the failure in the two adjacent phases 'a' and 'b' when the vectors V0, V1, V2 and V7 are implemented respectively.
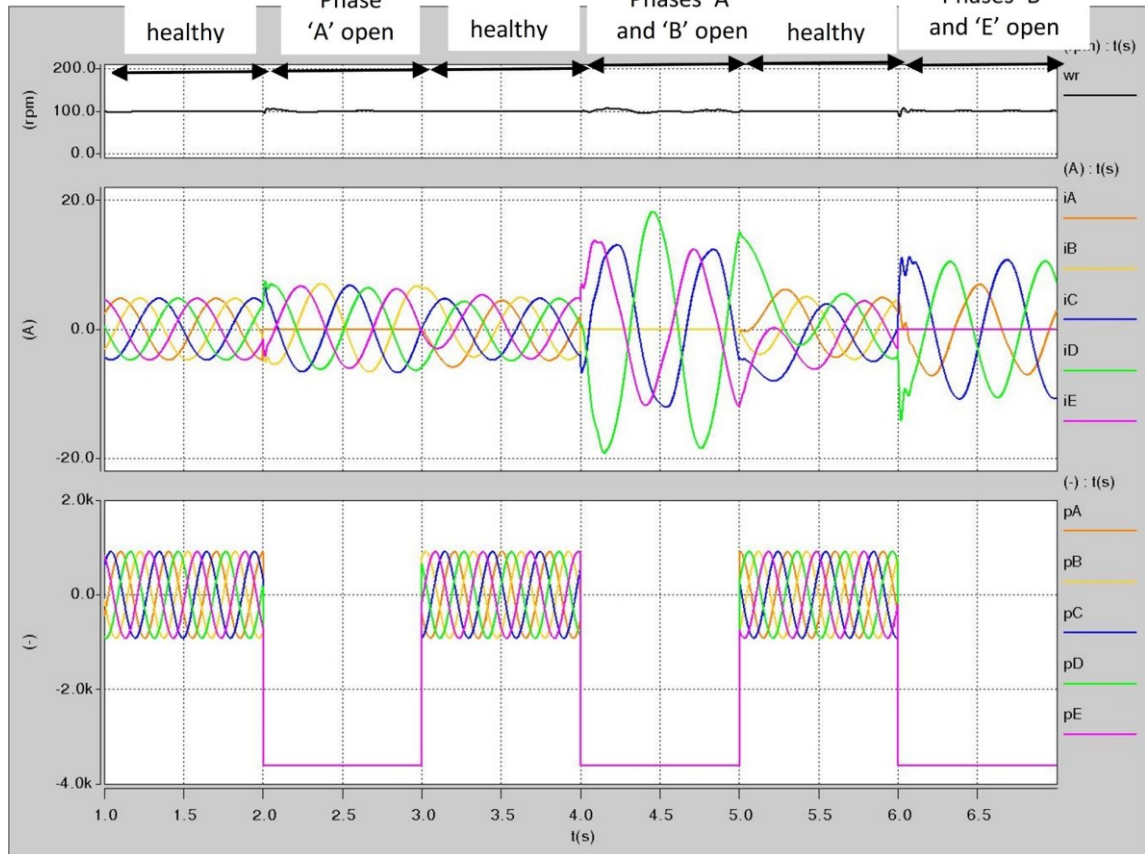

Figure 12 identify the saliency position under normal operating condition and post the failure according to [34-35].
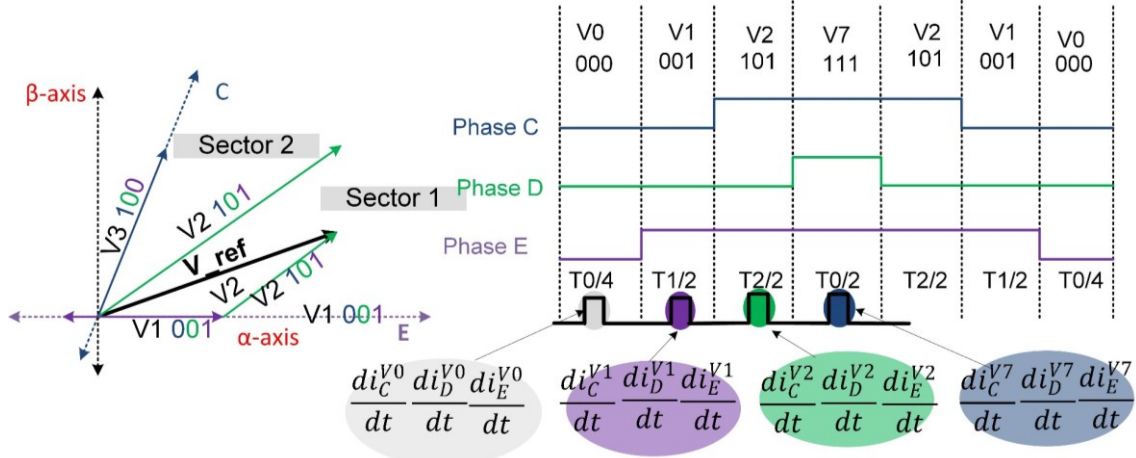

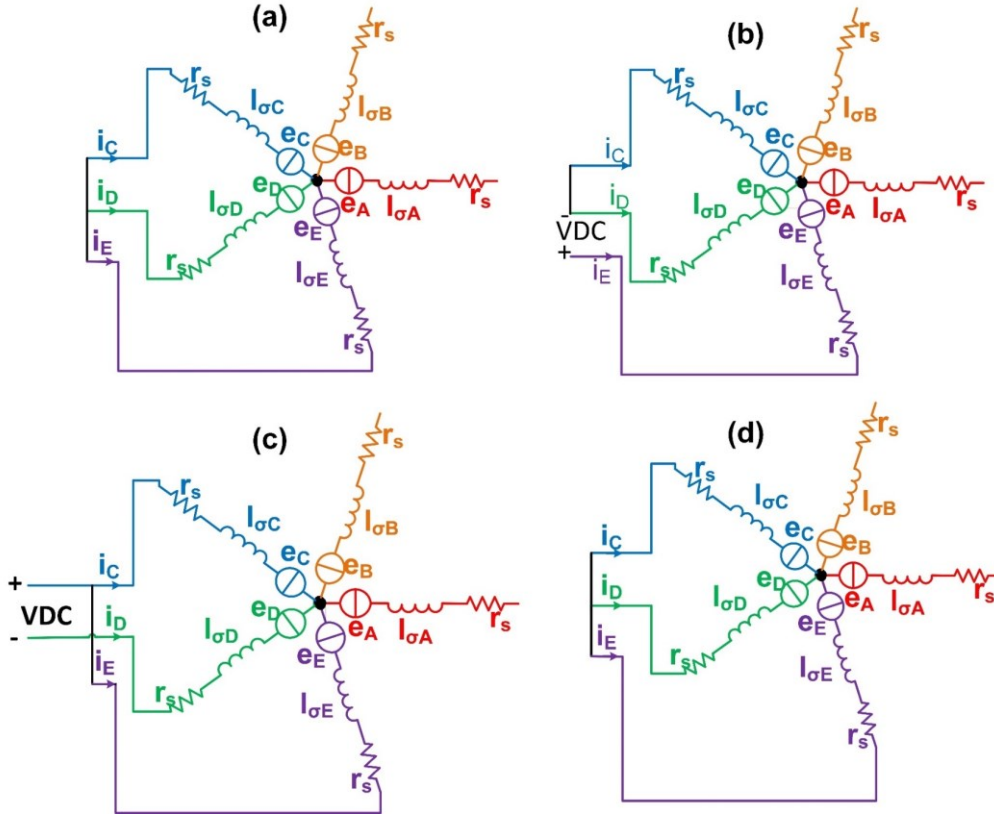*Figure 13. Sampling instant of the remaining currents post the failure in the two adjacent phases 'A' and 'B'.*

Figure14. Stator circuits when: (a) V0 is implanted , (b) V1 is implanted , (c) V2 is implanted ,(d) V7 is implanted

Using the circuits in Figures 14.a and figure 14.b, equation (14) can be derived:-

$$\begin{bmatrix} 0 \\ 0 \\ VDC \end{bmatrix} = r_s * \begin{bmatrix} i_C^{(V1)} - i_C^{(V0)} \\ i_D^{(V1)} - i_D^{(V0)} \\ i_E^{(V1)} - i_E^{(V0)} \end{bmatrix} + \begin{bmatrix} l_{\sigma C} * \dfrac{d}{dt}\left(i_C^{(V1)} - i_C^{(V0)}\right) \\ l_{\sigma D} * \dfrac{d}{dt}\left(i_D^{(V1)} - i_D^{(V0)}\right) \\ l_{\sigma E} * \dfrac{d}{dt}\left(i_E^{(V1)} - i_E^{(V0)}\right) \end{bmatrix} + \begin{bmatrix} e_C^{(V1)} - e_C^{(V0)} \\ e_D^{(V1)} - e_D^{(V0)} \\ e_E^{(V1)} - e_E^{(V0)} \end{bmatrix} \quad (14)$$

Where $l_{\sigma\,C,D,E}$ are the stator leakage inductances and $e_{C,D,E}$ are the back emf.
Equation (15) is obtained through using the circuits in figure 14.b and figure 14.c :-

$$\begin{bmatrix} VDC \\ 0 \\ 0 \end{bmatrix} = r_s * \begin{bmatrix} i_C^{(V2)} - i_C^{(V1)} \\ i_D^{(V2)} - i_D^{(V1)} \\ i_E^{(V2)} - i_E^{(V1)} \end{bmatrix} + \begin{bmatrix} l_{\sigma C} * \dfrac{d}{dt}\left(i_C^{(V2)} - i_C^{(V1)}\right) \\ l_{\sigma D} * \dfrac{d}{dt}\left(i_D^{(V2)} - i_D^{(V1)}\right) \\ l_{\sigma E} * \dfrac{d}{dt}\left(i_E^{(V2)} - i_E^{(V1)}\right) \end{bmatrix} + \begin{bmatrix} e_C^{(V2)} - e_C^{(V1)} \\ e_D^{(V2)} - e_D^{(V1)} \\ e_E^{(V2)} - e_E^{(V1)} \end{bmatrix} \quad (15)$$

Finally, equation (16) is derived using the circuits in figure 14.c and figure 14.d :-

$$\begin{bmatrix} 0 \\ VDC \\ 0 \end{bmatrix} = r_s * \begin{bmatrix} i_C^{(V7)} - i_C^{(V2)} \\ i_D^{(V7)} - i_D^{(V2)} \\ i_E^{(V7)} - i_E^{(V2)} \end{bmatrix} + \begin{bmatrix} l_{\sigma C} * \dfrac{d}{dt}\left(i_C^{(V7)} - i_C^{(V2)}\right) \\ l_{\sigma D} * \dfrac{d}{dt}\left(i_D^{(V7)} - i_D^{(V2)}\right) \\ l_{\sigma E} * \dfrac{d}{dt}\left(i_E^{(V7)} - i_E^{(V2)}\right) \end{bmatrix} + \begin{bmatrix} e_C^{(V7)} - e_C^{(V2)} \\ e_D^{(V7)} - e_D^{(V2)} \\ e_E^{(V7)} - e_E^{(V2)} \end{bmatrix} \quad (16)$$

At low speeds, the drop voltage across the stator resistance and back emf can be neglected. And hence the following equations can be obtained:-

$$\begin{bmatrix} pC \\ pD \\ pE \end{bmatrix} = \begin{bmatrix} \dfrac{di_C^{(V2)}}{dt} - \dfrac{di_C^{(V1)}}{dt} \\ \dfrac{di_D^{(V7)}}{dt} - \dfrac{di_D^{(V2)}}{dt} \\ \dfrac{di_E^{(V1)}}{dt} - \dfrac{di_E^{(V0)}}{dt} \end{bmatrix} \quad (17)$$

The saliency position scalars of the five phase PMSM motor post the failure of the two adjacent phases 'A' and 'B' in all sectors are given in table 5.

Sector no	pC	pD	pE
1	$\dfrac{di_C^{(V2)}}{dt} - \dfrac{di_C^{(V1)}}{dt}$	$\dfrac{di_D^{(V7)}}{dt} - \dfrac{di_D^{(V2)}}{dt}$	$\dfrac{di_E^{(V1)}}{dt} - \dfrac{di_E^{(V0)}}{dt}$
2	$\dfrac{di_C^{(V3)}}{dt} - \dfrac{di_C^{(V0)}}{dt}$	$\dfrac{di_D^{(V7)}}{dt} - \dfrac{di_D^{(V2)}}{dt}$	$\dfrac{di_E^{(V2)}}{dt} - \dfrac{di_E^{(V3)}}{dt}$
3	$\dfrac{di_C^{(V3)}}{dt} - \dfrac{di_C^{(V0)}}{dt}$	$\dfrac{di_D^{(V4)}}{dt} - \dfrac{di_D^{(V3)}}{dt}$	$\dfrac{di_E^{(V7)}}{dt} - \dfrac{di_E^{(V4)}}{dt}$
4	$\dfrac{di_C^{(V4)}}{dt} - \dfrac{di_C^{(V5)}}{dt}$	$\dfrac{di_D^{(V5)}}{dt} - \dfrac{di_D^{(V0)}}{dt}$	$\dfrac{di_E^{(V7)}}{dt} - \dfrac{di_E^{(V4)}}{dt}$
5	$\dfrac{di_C^{(V7)}}{dt} - \dfrac{di_C^{(V5)}}{dt}$	$\dfrac{di_D^{(V6)}}{dt} - \dfrac{di_D^{(V0)}}{dt}$	$\dfrac{di_E^{(V5)}}{dt} - \dfrac{di_E^{(V6)}}{dt}$
6	$\dfrac{di_C^{(V7)}}{dt} - \dfrac{di_C^{(V6)}}{dt}$	$\dfrac{di_D^{(V6)}}{dt} - \dfrac{di_D^{(V1)}}{dt}$	$\dfrac{di_E^{(V1)}}{dt} - \dfrac{di_E^{(V0)}}{dt}$

2.3.2 tracking the saliency post the failure in the non-adjacent phases 'B' and 'E'

Figure 15 shows the proposed SVPWM and the PWM waveform that is used as a part of the FTC strategy post the failure in the two nonadjacent phases 'B' and 'E' of the five-phase motor when the V_ref is located in the first sector.
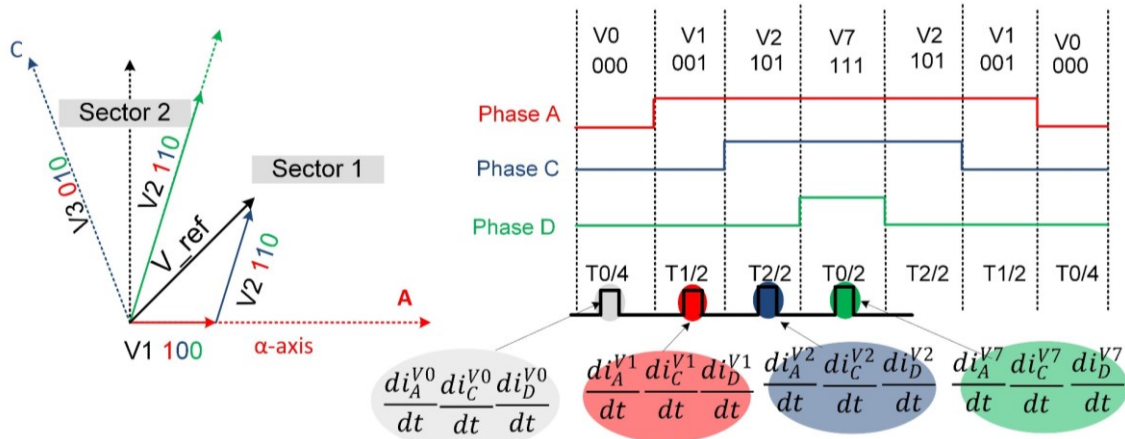

Figure 15. Sampling instant of the remaining currents post the failure in the two nonadjacent phases 'B' and 'E'

Figures 16.a, 16.b, 16.c, and 16.d show the stator circuits of five-phase PM motor under the failure in the two non-adjacent phases 'B' and 'E' when the vectors V0, V1, V2 and V7 are implemented respectively. Using the circuits in Figures 16.a and 16.b, equation (18) can be derived: -

$$\begin{bmatrix} VDC \\ 0 \\ 0 \end{bmatrix} = r_s * \begin{bmatrix} i_A^{(V1)} - i_A^{(V0)} \\ i_C^{(V1)} - i_C^{(V0)} \\ i_D^{(V1)} - i_D^{(V0)} \end{bmatrix} + \begin{bmatrix} l_{\sigma A} * \dfrac{d}{dt}\left(i_A^{(V1)} - i_A^{(V0)}\right) \\ l_{\sigma C} * \dfrac{d}{dt}\left(i_C^{(V1)} - i_C^{(V0)}\right) \\ l_{\sigma D} * \dfrac{d}{dt}\left(i_D^{(V1)} - i_D^{(V0)}\right) \end{bmatrix} + \begin{bmatrix} e_A^{(V1)} - e_A^{(V0)} \\ e_C^{(V1)} - e_C^{(V0)} \\ e_D^{(V1)} - e_D^{(V0)} \end{bmatrix} \quad (18)$$

Equation (19) is obtained through using the circuits in figures 16.b and 16.c:-

$$\begin{bmatrix} 0 \\ VDC \\ 0 \end{bmatrix} = r_s * \begin{bmatrix} i_A^{(V2)} - i_A^{(V1)} \\ i_C^{(V2)} - i_C^{(V1)} \\ i_D^{(V2)} - i_D^{(V1)} \end{bmatrix} + \begin{bmatrix} l_{\sigma A} * \dfrac{d}{dt}\left(i_A^{(V2)} - i_A^{(V1)}\right) \\ l_{\sigma C} * \dfrac{d}{dt}\left(i_C^{(V2)} - i_C^{(V1)}\right) \\ l_{\sigma D} * \dfrac{d}{dt}\left(i_D^{(V2)} - i_D^{(V1)}\right) \end{bmatrix} + \begin{bmatrix} e_A^{(V2)} - e_A^{(V1)} \\ e_C^{(V2)} - e_C^{(V1)} \\ e_D^{(V2)} - e_D^{(V1)} \end{bmatrix} \quad (19)$$
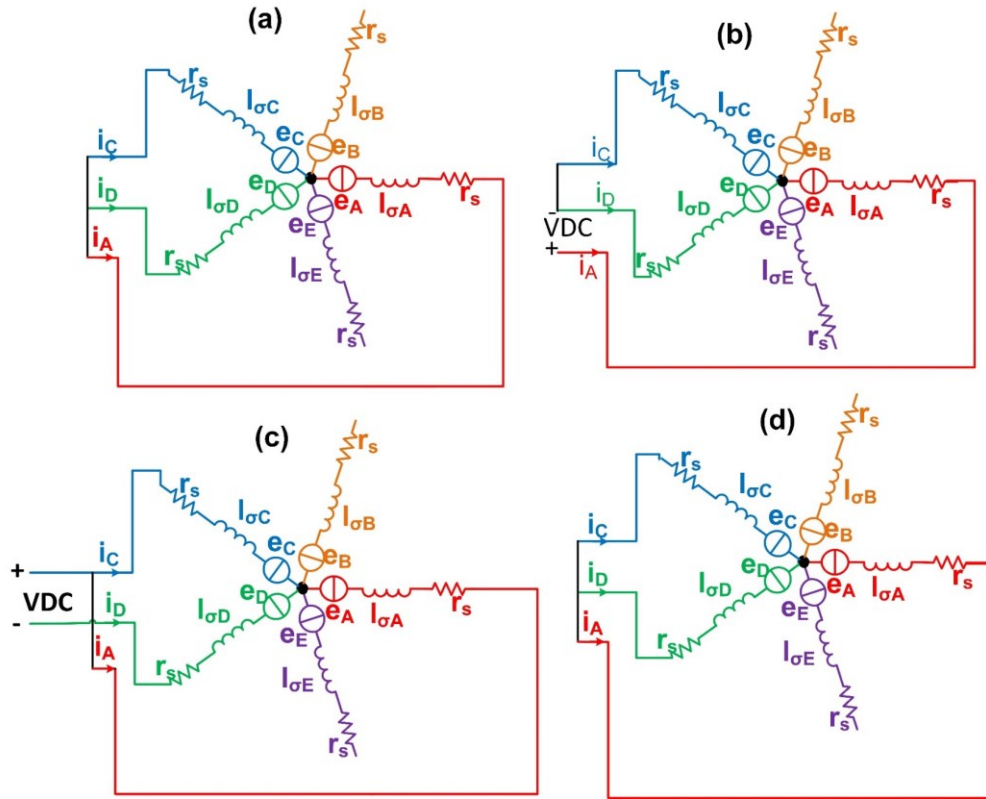
Figure 16. Stator circuits when: (a) V0 is applied (b) V1 is applied; (c) V2 is applied; (d) V7 is applied

Finally, equation (20) is derived using the circuits in figures 16.c and 16.d :-

$$\begin{bmatrix} 0 \\ 0 \\ VDC \end{bmatrix} = r_s * \begin{bmatrix} i_A^{(V7)} - i_A^{(V2)} \\ i_C^{(V7)} - i_C^{(V2)} \\ i_D^{(V7)} - i_D^{(V2)} \end{bmatrix} + \begin{bmatrix} l_{\sigma A} * \dfrac{d}{dt}\left(i_A^{(V7)} - i_A^{(V2)}\right) \\ l_{\sigma C} * \dfrac{d}{dt}\left(i_C^{(V7)} - i_C^{(V2)}\right) \\ l_{\sigma D} * \dfrac{d}{dt}\left(i_D^{(V7)} - i_D^{(V2)}\right) \end{bmatrix} + \begin{bmatrix} e_A^{(V7)} - e_A^{(V2)} \\ e_C^{(V7)} - e_C^{(V2)} \\ e_D^{(V7)} - e_D^{(V2)} \end{bmatrix} \quad (20)$$

By neglecting the voltage drop on the stator resistance and the back emf, the equation below can be written:
-

$$\begin{bmatrix} pA \\ pC \\ pD \end{bmatrix} = \begin{bmatrix} \dfrac{di_A^{(V1)}}{dt} - \dfrac{di_A^{(V0)}}{dt} \\ \dfrac{di_C^{(V2)}}{dt} - \dfrac{di_C^{(V1)}}{dt} \\ \dfrac{di_D^{(V7)}}{dt} - \dfrac{di_D^{(V2)}}{dt} \end{bmatrix} \quad (21)$$

The saliency position scalars of the five phase PMSM motor post the failure of the two non-adjacent phases 'B' and 'E' in all sectors are given in table 6 .

Table 6 T algorithm for identifying the saliency position post the failure in the nonadjacent phases 'B' and 'E'

Sector no	pA		pC		pD	
1	$\dfrac{di_A^{(V1)}}{dt}$	$-\dfrac{di_A^{(V0)}}{dt}$	$\dfrac{di_C^{(V2)}}{dt}$	$-\dfrac{di_C^{(V1)}}{dt}$	$\dfrac{di_D^{(V7)}}{dt}$	$-\dfrac{di_D^{(V2)}}{dt}$
2	$\dfrac{di_A^{(V2)}}{dt}$	$-\dfrac{di_A^{(V3)}}{dt}$	$\dfrac{di_C^{(V3)}}{dt}$	$-\dfrac{di_C^{(V0)}}{dt}$	$\dfrac{di_D^{(V7)}}{dt}$	$-\dfrac{di_D^{(V2)}}{dt}$
3	$\dfrac{di_A^{(V7)}}{dt}$	$-\dfrac{di_A^{(V4)}}{dt}$	$\dfrac{di_C^{(V3)}}{dt}$	$-\dfrac{di_C^{(V0)}}{dt}$	$\dfrac{di_D^{(V4)}}{dt}$	$-\dfrac{di_D^{(V3)}}{dt}$
4	$\dfrac{di_A^{(V7)}}{dt}$	$-\dfrac{di_A^{(V4)}}{dt}$	$\dfrac{di_C^{(V4)}}{dt}$	$-\dfrac{di_C^{(V5)}}{dt}$	$\dfrac{di_D^{(V5)}}{dt}$	$-\dfrac{di_D^{(V0)}}{dt}$
5	$\dfrac{di_A^{(V6)}}{dt}$	$-\dfrac{di_A^{(V5)}}{dt}$	$\dfrac{di_C^{(V7)}}{dt}$	$-\dfrac{di_C^{(V6)}}{dt}$	$\dfrac{di_D^{(V5)}}{dt}$	$-\dfrac{di_D^{(V0)}}{dt}$

| 6 | $\dfrac{di_A^{(V1)}}{dt} - \dfrac{di_A^{(V0)}}{dt}$ | $\dfrac{di_C^{(V7)}}{dt} - \dfrac{di_C^{(V6)}}{dt}$ | $\dfrac{di_D^{(V6)}}{dt} - \dfrac{di_D^{(V1)}}{dt}$ |

2.3.3   *Simulation results for the saliency tracking post the failure in two phases*

The algorithm to identify the saliency position of the five-phase motor post the failure in the two adjacent phases 'A' and 'B' and the two non-adjacent phases 'B' and 'E' was simulated in Saber and the results are shown in figure 17 where plafa and pbeta are alfa and beta components of the position signals. The results demonstrate the ability of the proposed algorithms to track the saliency post the failure of the two phases in the same quality that is obtained under the normal operating conditions and post the failure in phase 'A' .
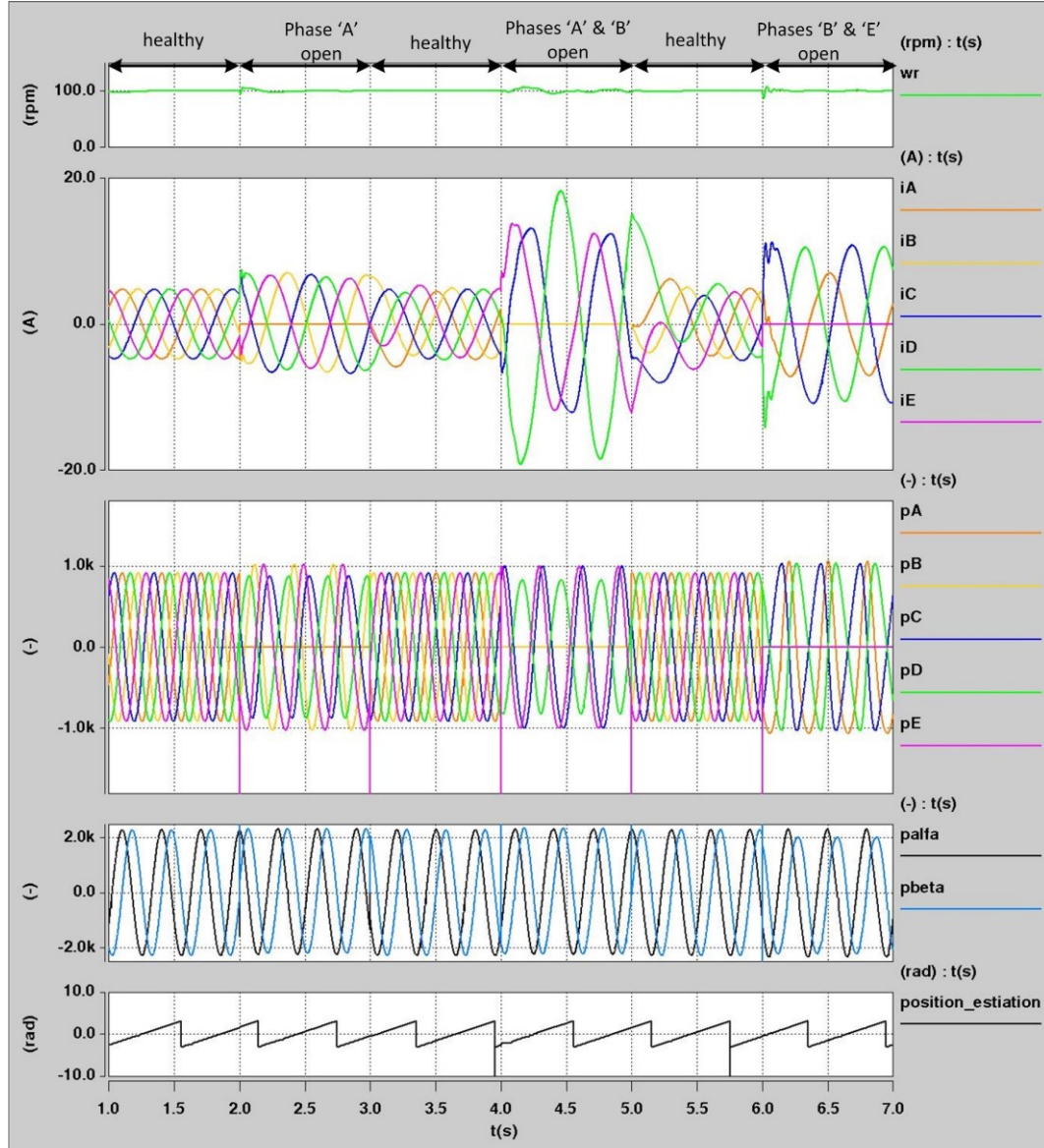
Figure 17 Identifying the saliency position post the fault the two phase failure using the proposed algorithms.

2.4 *Speed control post the failure in two phases and post the failure in speed sensor*

The speed control structure that was utilized in the paper to control the five-phase PMSM post the failure in the two phases and the failure in the speed sensor occurred simultaneously is shown in figure 18. The SVPWM technique is changed and hence the saliency tracking algorithm is based on the status of the five-phase motor. For example, if the motor is running under the normal operating conditions, then, the symmetric SVPWM will be implemented and at the same time, the algorithm proposed in [36-37] will be used to track the saliency. While the Asymmetric SVPWM and the associated saliency tracking algorithm will be used in the case of a fault in phase 'A' [38-39]. Finally, the new SVPWM techniques and saliency tracking algorithms proposed in

this work will be used post the failures in the adjacent phase 'A' and 'B' and the nonadjacent phase 'B' and 'E' respectively. A mechanical observer was used in this work to obtain a filtered speed signal $\omega r^{\wedge}$ and a filtered position $\theta r^{\wedge}$[40]. The outputs of the mechanical observer were used as a feedback signal post the failure in the spe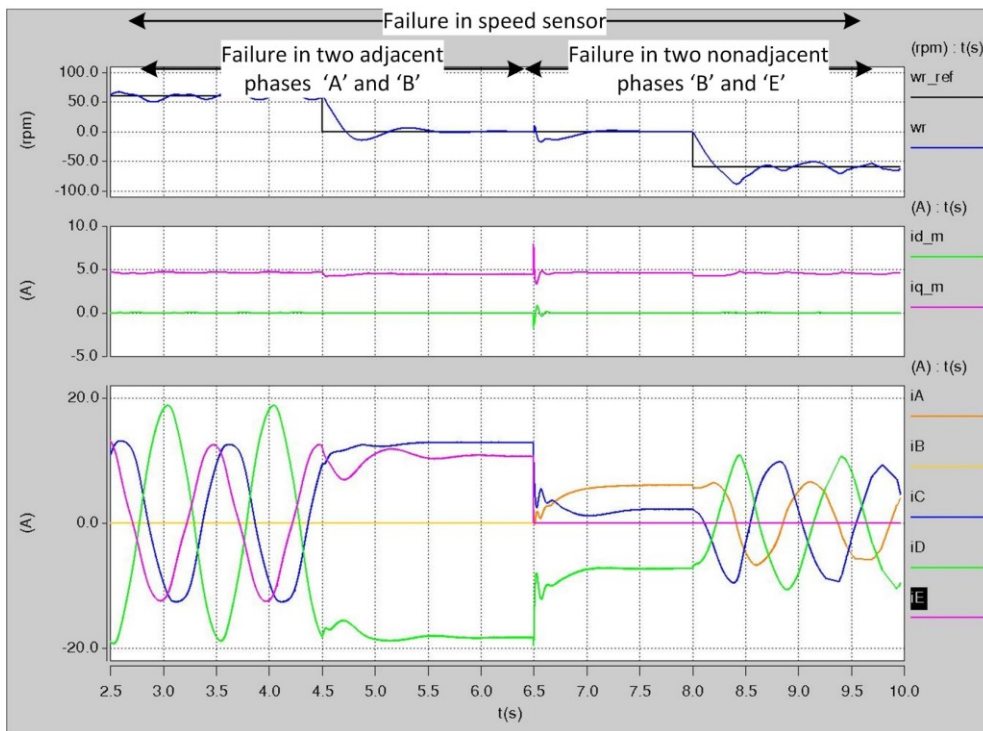ed sensor as shown in figure 18. And to make the simulation more realistic, a 10 us a minimum pulse width were made di/dt is sampled.

Figure 18 speed control structure post the failure in the two adjacent phase and the failure in the speed sensor occurred simulatenously.

Figure 19, figure 20, and figure 21 show the performance of the five-phase PMSM drive at different conditions post the failures. Figure 19, shows the low-speed operation of the PMSM drive under the failure of two-phase and the failure of the speed sensor occurred simultaneously. During the time period [2.5s-6.5s] the motor was running post the failure in the two adjacent phases 'A' and 'B' and the failure in the speed sensor at the same time. Also, the reference speed was changed from 30 rpm to zero in this period at t=4.5s. During the time period [6.5s-10s] the motor was running post the failure in two non-adjacent phases 'B' and 'E' and the failure in the speed sensor. Moreover, the reference speed was changed from 0 rpm to -30 rpm in this period 8s. Figure 19 shows that the performance of the whole system post the failure in the two phases of the motor and post the failure in the speed sensor occurred simultaneously is as good as that obtained for the motor running without faults.

Figure 19 low-speed operation post the failure in two phase and failure in the speed sensor.

Figure 20 demonstrates the performance of the system when high-speed steps were implemented to the drive system post the failure in two phases and the failure in the speed sensor occurred simultaneously.   The results show that the motor responded to the speed steps (from 250 rpm to 0 and to 250 rpm) without compromising the dynamic and steady-state performance.
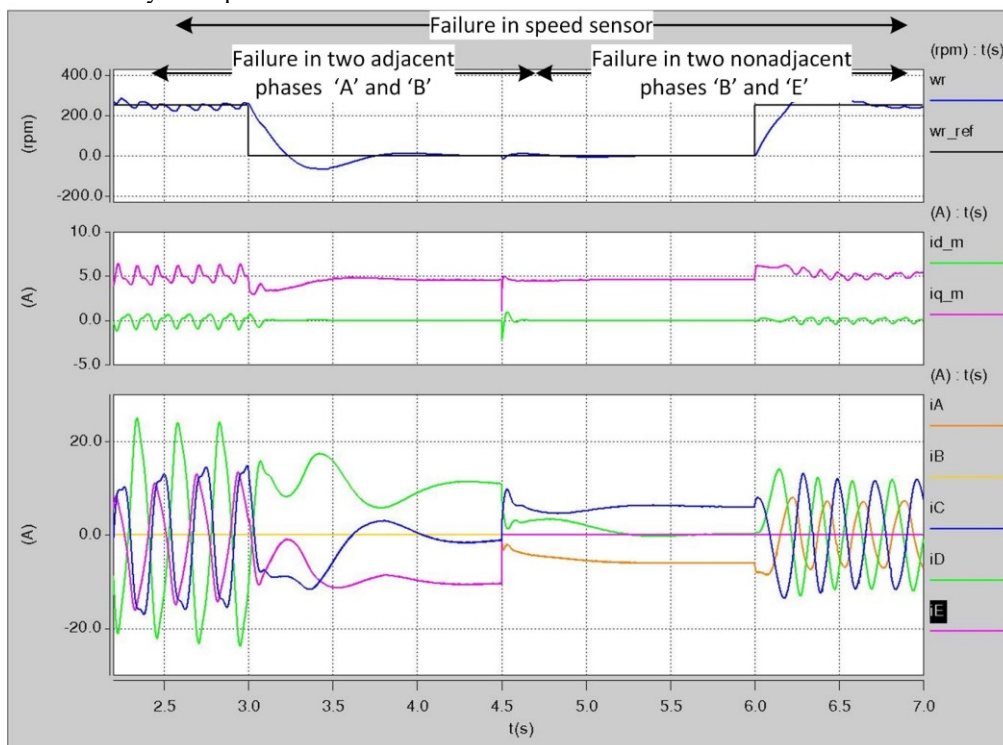

Figure 20 High-speed operation post the failure in two phase and the failure in the speed sensor.

Figure 21 shows the stability of the system to maintain the speed during the load disturbance post the failure in two phases and the failure in the speed sensor occurred simultaneously. The results show that the system maintains the speed in all the cases.
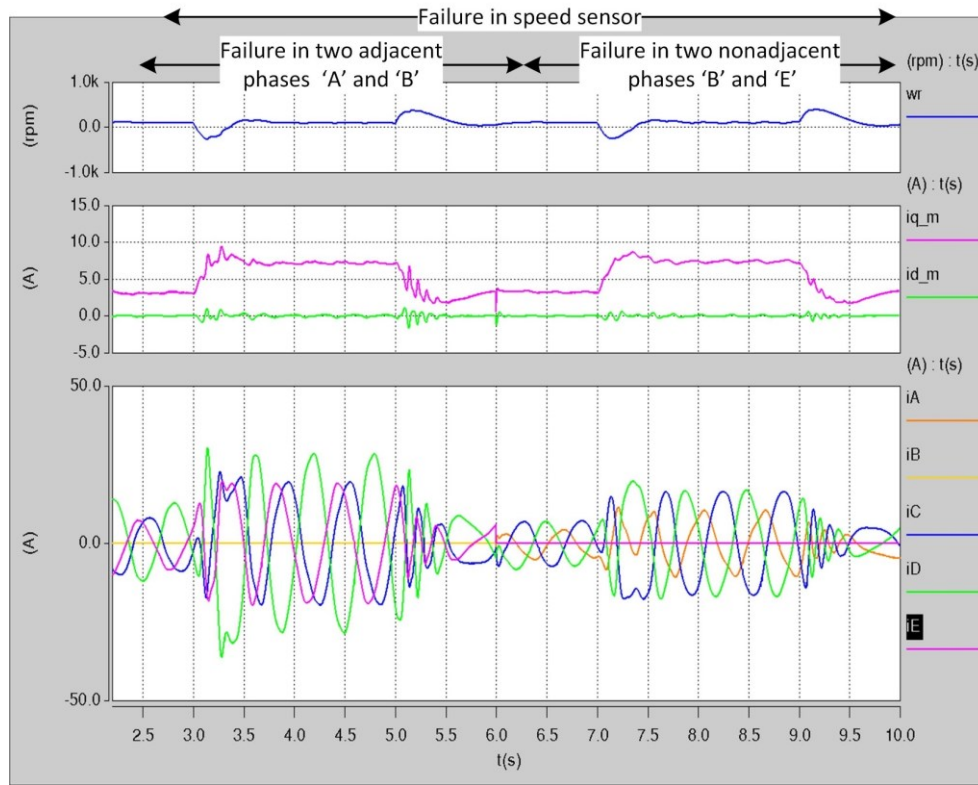
Figure 21 Load steps operation post the failure in two phase and the failure in the speed sensor.

3. Conclusion

This paper has proposed a novel control technique to maintain the operation of the five-phase PMSM post the failure in two phases of the motor and post the failure of the speed sensor occurred simultaneously. This control technique is including an FTC strategy based on using new SVPWM techniques and also including an algorithm to identify the saliency position post the failure. The results have shown the reliability of this technique to maintain the performance of the PMSM drive with low torque ripple at different load conditions post the failure. The implementation of this technique is quite easy.

4. Appendices

The dwell time under two adjacent phases are calculated using figure 13. The figure illustrate how the adjacent vectors (V1=001, V2= 101, and V0=111) are utilized to generate the reference voltage (V_ref) if it is located in the first sector. The duration of applying the vectors V1,V2 and V0 i.e (T1/4, T2/2, and T0/4) can be obtained as follows :-

$$V_\alpha * Ts = V1 * T1 + V2 * T2 * \cos\ (\theta_x) = 0.4*\text{VDC}*\text{T1}+1.618*0.4*\text{VDC}*\text{T2}* \cos\ (\theta_x) \quad (22)$$

$$V_\beta * Ts = V2 * T2 * \sin\ (\theta_x) = 1.618*0.4*\text{VDC}*\text{T2}* \sin\ (\theta_x) \quad (23)$$

From equations (22,23) the dwell time in the first sector can be calculated as shown below:-

$$T2 = \frac{V_\beta}{1.618*0.4*VDC*\sin\ (\theta_x)} * Ts \quad (24)$$

$$T2 = \frac{V_\alpha*\tan(\theta_x)-V_\beta}{0.4*VDC*\tan\ (\theta_x)} * Ts \quad (25)$$

The same procedure can be done for the other sectors and also when the fault is occurred in the two non adjacent phases.

References

[1] Villani, M., Tursini, M., Fabri, G. & Castellini, L. (2010, December). Multi-phase fault tolerant drives for aircraft applications. In Electrical Systems for Aircraft, Railway and Ship Propulsion conference (pp. 1-6). Bologna, Italy.

[2] H. T. Canseven and A. Ünsal, "Performance Improvement of a Five-Phase PMSM Drive Under Open Circuit Stator Faults," 2021 5th International Symposium on Multidisciplinary Studies and Innovative Technologies (ISMSIT), 2021, pp. 561-565, doi: 10.1109/ISMSIT52890.2021.9604537.

[3] Chen, K. (2015, June). Multiphase pulse-width modulation considering reference order for sinusoidal wave production. In IEEE 10th Conference on Industrial Electronics and Applications (ICIEA) (pp. 1155-1160). Auckland, New Zealand,.

[4] Xue, S., Wen, X., & Feng, Z. (2006, August). A Novel Multi-Dimensional SVPWM Strategy of Multiphase Motor Drives. In 12th International Power Electronics and Motion Control Conference (pp. 931-935). Shanghai, China .

[5] Wang, P., Zheng., P., Wu, F., Zhang, J. & Li, T. (2014, August). Research on dual-plane vector control of fivephase fault-tolerant permanent magnet machine. in IEEE Conference and Expo Transportation Electrification Asia-Pacific (ITEC Asia-Pacific) (pp. 1-5). Beijing, China.

[6] Parsa, L. & Toliyat, H. (2007). Sensorless Direct Torque Control of Five-Phase Interior Permanent-Magnet Motor Drives. IEEE Transactions on Industry Applications. 43, 4, pp. 952-959.

[7] Bianchi, N., Bolognani, S. & Dai Pre, M. (2007). Strategies for the Fault-Tolerant Current Control of a Five-Phase Permanent-Magnet Motor. IEEE Transactions on Industry Applications. 43,4, pp. 960-970.

[8] Mohammadpour, A., Sadeghi, S., & Parsa, L. (2014). A Generalized Fault-Tolerant Control Strategy for Five-Phase PM Motor Drives Considering Star, Pentagon, and Pentacle Connections of Stator Windings. *Industrial Electronics, IEEE Transactions on.* 61, pp. 63-75.

[9] Abdel-Khalik, A., Ahmed, S., Elserougi, A., & Massoud, A. (2015). Effect of Stator Winding Connection of Five-Phase Induction Machines on Torque Ripples Under Open Line Condition. Mechatronics, IEEE/ASME Transactions on. 20, pp. 580-593.

[10] Sedrine, E., Ojeda, J., M. Gabsi, M., & Slama-Belkhodja, I. (2015). Fault-Tolerant Control Using the GA Optimization Considering the Reluctance Torque of a Five-Phase Flux Switching Machine. in IEEE Transactions on Energy Conversion, 30, 3, pp. 927-938.

[11] B. Tian, J. Hu, X. Huang, B. Zhou and Q. An, "Performance comparison of three types of PWM techniques for a Five-phase PMSM with a single-phase open circuited," 2021 13th International Symposium on Linear Drives for Industry Applications (LDIA), 2021, pp. 1-5, doi: 10.1109/LDIA49489.2021.9505984..

[12] Chen, Q., Liu, G., Zhao, W., Qu, L. & Xu, G. (2017). Asymmetrical SVPWM Fault-Tolerant Control of Five-Phase PM Brushless Motors. *IEEE Transactions on Energy Conversion*. 32, 1, pp. 12-22.

[13] Guzman, H., Duran, M., Barrero, F., Zarri, L., Bogado, B., Prieto, I. & Arahal, M. (2016). Comparative study of predictive and resonant controllers in fault-tolerant five-phase induction motor drives. IEEE Transactions on Industrial Electronics. 63, 1, pp. 606–617.

[14] Cheng, L., Sui, Y., Zheng, P., Wang, P., & Wu, F. (2018). Implementation of postfault decoupling vector control and mitigation of current ripple for five-phase fault-tolerant PM machine under single-phase open-circuit fault. IEEE Trans. Power Electron., 33, 10, pp. 8623–8636.

[15] Zhou, H., Zhao, W., Liu, G., Cheng, R., & Xie, Y. (2017). Remedial field-oriented control of five-phase fault-tolerant permanent-magnet motor by using reduced-order transformation matrices. In IEEE Trans. Ind. Electron., 64, 1, pp. 169–178.

[16] Chen, Q., Zhao, W., Liu, G., & Lin, Z. (2019). Extension of virtual-signal injection-based MTPA control for five-phase IPMSM into fault-tolerant operation. In IEEE Trans. Ind. Electron., 66, 2, pp. 944–955.

[17] Chen, Q., Gu, L., Lin, Z., & Liu, G. (2020). Extension of space-vector signal-injection-based MTPA control into SVPWM fault-tolerant operation for five-phase IPMSM. In IEEE Trans. Ind. Electron., 67, 9, pp. 7321–7333.

[18] B. Tian, M. Molinas and Q. An, "PWM Investigation of a Field-Oriented Controlled Five-Phase PMSM Under Two-Phase Open Faults," in IEEE Transactions on Energy Conversion, vol. 36, no. 2, pp. 580-593, June 2021, doi: 10.1109/TEC.2020.3029264.

[19] Liu, G., Lin, Z., Zhao, W., Chen, Q., & Xu,G. (2018). Third harmonic current injection in fault-tolerant five-phase permanent-magnet motor drive. In IEEE Trans. Power Electron., 33, 8, pp. 6970–6979.

[20] Xiong, C., Guan, T., Zhou, P., & Xu, H. (2020). A fault-tolerant FOC strategy for five-phase SPMSM with minimum torque ripples in the full torque operation range under double-phase open-circuit fault. In IEEE Trans. Ind. Electron., 67, 11, pp. 9059–9072.

[21] Bermudez, M., Gonzalez-Prieto, I., Barrero, F., Guzman, H., Kestelyn, X., & Duran, m. (2018). An Experimental Assessment of Open-Phase Fault-Tolerant Virtual-Vector-Based Direct Torque

Control in Five-Phase Induction Motor Drives. In IEEE Transactions on Power Electronics, 33, 3, pp. 2774-2784.

[22] Tian, B., Mirzaeva, G., An, Q., Sun, L., & Semenov, D. (2018). Fault-Tolerant Control of a Five-Phase Permanent Magnet Synchronous Motor for Industry Applications. In IEEE Transactions on Industry Applications, 54, 4, pp. 3943-3952.

[23] Huang, W., Hua, W., Chen, F., Yin, F., & Qi, J. (2018). Model Predictive Current Control of Open-Circuit Fault-Tolerant Five-Phase Flux-Switching Permanent Magnet Motor Drives. In IEEE Journal of Emerging and Selected Topics in Power Electronics,6,4, pp. 1840-1849.

[24] L. Zheng, J. E. Fletcher, B. W. Williams, and X. He, ''A novel direct torque control scheme for a sensorless five-phase induction motor drive,'' IEEE Trans. Ind. Electron., vol. 58, no. 2, pp. 503–513, Feb. 2011.

[25] L. Zhang, Y. Fan, C. Li, A. Nied, and M. Cheng, ''Fault-tolerant sensorless control of a five-phase FTFSCW-IPM motor based on a wide-speed strongrobustness sliding mode observer,'' IEEE Trans. Energy Convers., vol. 33, no. 1, pp. 87–95, Mar. 2018.

[26] A. H. Almarhoon, Z. Q. Zhu, and P. Xu, ''Improved rotor position estimation accuracy by rotating carrier signal injection utilizing zero-sequence carrier voltage for dual three-phase PMSM,'' IEEE Trans. Ind. Electron., vol. 64, no. 6, pp. 4454–4462, Jun. 2017

[27] G. Liu, C. Geng and Q. Chen, "Sensorless Control for Five-Phase IPMSM Drives by Injecting HF Square-Wave Voltage Signal into Third HarmonicSpace," in *IEEE Access*, vol. 8, pp. 69712-69721, 2020, doi:10.1109/ACCESS.2020.2986347.

[28] Saleh, K., Sumner, M. Sensorless Speed Control of Five-Phase PMSM Drives in Case of a Single-Phase Open-Circuit Fault. *Iran J Sci Technol Trans Electr Eng* **43,** 501–517 (2019).

[29] B. Tian, M. Molinas, Q. An, B. Zhou and J. Wei, "Freewheeling current-based sensorless field-oriented control of Five-Phase PMSMs under IGBT failures of a single phase," in *IEEE Transactions on Industrial Electronics*, doi: 10.1109/TIE.2021.3053891.

[30] Hyung-Min, R., Ji-Woong, K. & Seung-Ki, S. (2004, October). Synchronous frame current control of multi-phase synchronous motor - part ii asymmetric fault condition due to open phases. in Industry Applications Conference of 39th IAS Annual Meeting(p. 275). Seattle,USA.

[31] Fu, J.R & Lipo T.A. (1994). Disturbance-free operation of a multiphase current-regulated motor drive with an opened phase. IEEE Trans. Ind. Appl. 30, 5, pp. 1267– 1274.

[32] Zhang, W., Xu, D., Enjeti, P., Li, H., Hawke, J. & Krishnamoorthy, H. (2014). Survey on Fault-Tolerant Techniques for Power Electronic Converters. Power Electronics, IEEE Transactions on. 29, 12, pp.6319,6331.

[33] Tani, A., Mengoni, M., Zarri, L., Serra G. & Casadei, D. (2012). Control of multi-phase induction motors with an odd number of phases under open circuit faults. IEEE Trans. Power Electron.27, 2, pp. 565–577.

[34] Nicola Bianchi, Silverio Bolognani and Michele Dai Pré, "Impact of Stator Winding of a Five-Phase Permanent Magnet Motor on Post-Fault Operations", in IEEE Trans. on Industry Electronics, IE, Vol. 55, No. 5, May 2008, Special Session on "Multiphase Machines and Drives", pp. 1978-1987.

[35] Nicola Bianchi, Silverio Bolognani, and Emanuele Fornasiero, "Performance of Five-Phase Motor Drive Under Post-Fault Operations" , in Electric Power Components and Systems, Taylor and Francis Ltd, Vol. 39, No. 12, Aug. 2011, pp. 1302-1314.

[36] K.Saleh and M.Sumner. Modelling and simulation of a sensorless control of fve phase PMSM drives using multi dimension space vector modulation. In: TELKOMNIKA (telecommunication, computing, electronics and control). 2016. Vol 14, No 4. pp 1269-1283. doi.org/10.12928/TELKOMNIKA.v14i4.3996.

[37] K.saleh and M.Sumner , Sensorless speed control of five-phase PMSM drives with low current distortion. Springer Electrical engineering journal. June 2018, Volume 100, Issue 2, pp 357–374. doi.org/10.1007/s0020.

[38] Saleh, K., Sumner, M. Sensorless Speed Control of Five-Phase PMSM Drives in Case of a Single-Phase Open-Circuit Fault. *Iran J Sci Technol Trans Electr Eng* **43,** 501–517 (2019). https://doi.org/10.1007/s40998-018-00173-4

[39] Kamel Saleh & Mark Sumner (2020) Sensorless Speed Control of a Fault-Tolerant Five-Phase PMSM Drives, Electric Power Components and Systems, 48:9-10, 919-932, DOI: 10.1080/15325008.2020.1825555

[40]] Lorenz RD, Van Patten KW. High-resolution velocity estimation for all-digital, ac servo drives. IEEE T Ind Appl 1991;27:701–705